JOURNAL OF GEOPHYSICAL RESEARCH, VOL. 93, NO. B5, PAGES 4745–4757, MAY 10, 1988

Stabilization of Rapid Frictional Slip on a Weakening Fault by Dilatant Hardening

JOHN W. RUDNICKI AND CHAO-HSUN CHEN

Department of Civil Engineering, Northwestern University, Evanston, Illinois

Frictional slip is often accompanied by dilatancy due to uplift in sliding over asperities and microcracking in the adjacent material. If dilatancy occurs more rapidly than pore fluid can flow into the newly created void space, the local pore pressure is reduced and the effective normal stress is increased in compression, tending to inhibit further slip. This dilatant hardening is analyzed for a simple model. One surface of a slab is loaded by compressive stress and shear displacement and connected to a reservoir of pore fluid held at constant pressure. The other boundary is a frictional surface, assumed to have formed at peak stress, on which the shear stress decreases from a peak value τ_p to a residual value τ_r as slip increases from zero to δ_0. In the absence of pore fluid effects an instability corresponding to an unbounded slip rate occurs when the slope of the shear stress versus slip relation is more negative than the unloading stiffness of the surrounding material. Dilatant hardening prevents this instability provided that the pore pressure in the reservoir is high enough. If the pressure in the reservoir is too low, the pressure at the fault surface can be reduced to the point at which the pore fluid bulk modulus decreases rapidly, eliminating the stabilizing effect. When the analysis is modified to include normal stress changes simulating those in the axisymmetric compression test, the prediction of the critical pressure in the reservoir agrees to within a factor of 2 or 3 with that observed by Martin in tests on Westerly granite. The predictions are also consistent with the trends observed by Martin of decreasing critical reservoir pore pressure with increasing effective confining stress and decreasing nominal strain rate.

INTRODUCTION

Dilatancy, or an increase in void volume, is typically associated with the inelastic deformation of relatively intact rock. However, dilatancy associated with frictional sliding in laboratory samples has also been observed by several workers [*Barton*, 1976; *Jamison and Teufel*, 1979; *Teufel*, 1981]. At low normal stresses, dilatancy may be due to uplift in sliding over asperity contacts. At higher normal stresses, dilatancy appears to result from the initiation and extension of microcracks adjacent to the sliding surface. If the rock is fluid saturated and dilatancy occurs more rapidly than pore fluid can diffuse into the newly created void space, the local pore pressure near the sliding surface decreases. This decrease in pore pressure increases the effective compressive stress (total compressive stress minus the pore fluid pressure) and inhibits further frictional slip. This paper investigates the stabilization that can result from coupling between pore fluid diffusion and dilatancy accompanying friction sliding. Specifically, we address whether the magnitude and duration of this stabilization are sufficient to be consistent with laboratory observations.

This paper is an outgrowth of previous work by *Rudnicki* [1984] which examined the effects of dilatant hardening on the development of concentrated strain in a narrow zone that was slightly weaker than the surrounding material. He found that dilatant hardening delayed the onset of an instability compared with its occurrence in the absence of pore fluid. The time duration of this delay was, however, very short: less than a few hours for tectonic strain rates and less than a few tens of seconds for typical laboratory strain rates. More specifically, this prediction for the delay time is much shorter than the several hundred seconds observed by *Martin* [1980] in pore fluid stabilization of failure in axially symmetric compression of Westerly granite.

One possible explanation for this discrepancy is the difference in deformation states. *Martin*'s [1980] experiments were conducted in axially symmetric compression, whereas *Rudnicki*'s [1984] analysis was for plane strain shear. Theoretical predictions of localization [*Rudnicki and Rice*, 1975] suggest that plane strain deformation states are more favorable for localization than axisymmetric ones, but whether these differences affect stabilization due to coupling between deformation and diffusion is unknown. *Rudnicki* [1983] has generalized the analysis for pure shear [*Rudnicki*, 1984] to arbitrary deformation states and has shown that the character of the response in axisymmetric compression is similar to that in pure shear, but no detailed calculations for the delay time were carried out.

Another, perhaps more likely explanation is that the stabilization observed by *Martin* [1980], or at least some of it, occurred after the deformation had already concentrated into a narrow zone and was associated with frictional sliding on a fault surface. Hence the stabilization occurs after the processes of localization analyzed by *Rudnicki* [1984]. The work to be described here assesses this possibility. In particular, we assume that a fault has formed at peak stress and that subsequent inelastic deformation in the postpeak region occurs entirely by frictional sliding on a well-defined surface with elastic unloading in the surrounding material. This assumption is consistent with the previous analysis of *Rudnicki* [1984] and with laboratory observations which typically indicate fault formation in the vicinity of peak stress, although frequently slightly before or after. Furthermore, these assumptions are also consistent with those made in analyses by *Rice* [1980] and *Wong* [1982] to extract shear fracture energies from observations of postpeak deformation. However, the details of the process by which a fault develops from a relatively homogeneous pattern of deformation are not well understood. Fortunately, knowledge of these details is not essential to this analysis. It suffices to assume that the deformation has been

Paper number 7B2067.
0148-0227/88/007B-2067$05.00

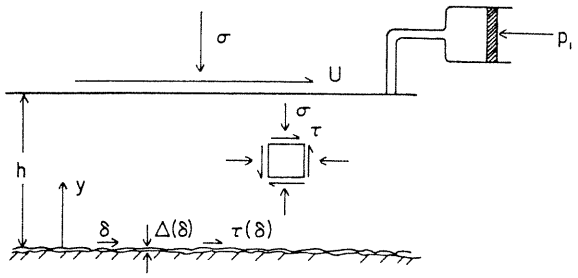

Fig. 1. Geometry of the problem. An infinite slab occupying $0 \le y \le h$ is loaded at $y = h$ by a horizontal displacement U and a prescribed normal stress σ. A fluid reservoir maintained at constant pressure p_1 is connected to the slab at $y = h$. The relative slip at $y = 0$ is δ, and the accompanying dilatancy is $\Delta(\delta)$. The stresses developed in the layer are a shear stress τ, a normal stress σ, and whatever reaction stresses are needed to maintain zero deformation in planes perpendicular to the y direction.

concentrated into a narrow zone having a thickness that is much less than other dimensions of the sample and that the deformation of the zone is effectively described by a relation between stress and relative displacement across the boundaries of the zone. Dilatancy, due to either uplift or near-fault microcracking, is assumed to accompany frictional slip and, by means of the mechanism described above, stabilize rapid slip.

A major simplifying assumption of the analysis is that the flow of pore fluid into the dilated fault surface is simply proportional to the difference between the pore pressure at the fault surface and that in a reservoir connected to the exterior of the sample. A more typical assumption would be that the fluid mass flow is proportional to the gradient of the pore fluid pressure as in Darcy's law. These two assumptions agree only in the limit of steady state flow, but the additional complications introduced by Darcy's law seem unwarranted in view of the scant observational evidence available.

FORMULATION

We consider a simple one-dimensional model consisting of a long slab (Figure 1) loaded at its top surface ($y = h$) by a shear displacement U and by a normal stress σ. A reservoir of pore fluid maintained at a constant pressure p is also connected to the slab at $y = h$. The slab is bounded at $y = 0$ by a fault or frictional surface assumed to have formed at peak shear stress. Both U and σ are taken to be zero at peak stress. The stresses developed in the layer are a shear stress τ, a normal stress σ, and whatever reaction stresses are needed to maintain zero deformation in planes perpendicular to the y direction. Because any spatial dependence is only on y, stress equilibrium requires that

$$\partial\tau/\partial y = 0 \qquad \partial\sigma/\partial y = 0 \tag{1}$$

and hence τ and σ are uniform throughout the slab.

For constant normal stress and pore pressure the shear stress on the frictional surface τ is related to the relative slip δ by

$$\tau = \tau_p - (\tau_p - \tau_r)g(\delta/\delta_0) \tag{2}$$

where τ_p is the peak shear stress, τ_r is the residual shear stress, and $g(\delta/\delta_0)$ is a function that describes the decrease of τ from τ_p to τ_r (Figure 2*a*). Specifically, $g(0) = 0$, and $g(1) = 1$. Equation (2) applies for $\delta \le \delta_0$; for $\delta > \delta_0$, $\tau = \tau_r$. Thus τ decreases from a peak value τ_p to a residual value τ_r as the slip increases from zero to δ_0. Although this form neglects time-dependent effects [e.g., *Dieterich*, 1978, 1979*a*, *b*, 1981; *Ruina*, 1980, 1983], which are small in magnitude but important in governing the stability of slip, it is consistent with τ versus δ curves inferred from axisymmetric compression experiments by *Rice* [1980] and *Wong* [1982] and those observed in shear tests by *Dieterich* [1978] and *Barton* [1972, 1973]. The simplest form for $g(x)$ that connects τ smoothly to τ_p and τ_r is the following:

$$g(x) = -2x^3 + 3x^2 \qquad 0 \le x \le 1 \tag{3}$$

If the normal stress and pore pressure are not constant, then a term proportional to the effective compressive stress must be added to (2) (Figure 2*b*). For frictional slip the appropriate expression for the effective stress is simply the difference between the total compressive stress and the pore fluid pressure. This form has a rational basis for frictional slip on surfaces with sharp, isolated asperity contacts [*Rice*, 1977]. Thus (2) becomes

$$\tau = \tau_p - (\tau_p - \tau_r)g(\delta/\delta_0) + m_0[\sigma - (p_0 - p_1)] \tag{4}$$

where σ is the total normal stress measured from its value at peak shear stress, p_0 is the value of the pore pressure at $y = 0$, and p_1 is its initial value. The friction coefficient m_0 will, in general, depend on both the amount of slip and on the effective normal stress [*Wong*, 1986] but here will be taken as constant.

Dilatancy is assumed to accompany frictional slip according to a relation of the following form:

$$\Delta = \Delta_0 f(\delta/\delta_0) \tag{5}$$

where $f(0) = 0$, $f(1) = 1$, and $\Delta = \Delta_0$ for $\delta > \delta_0$. Thus the maximum amount of dilatancy Δ_0 is achieved when the shear stress has been reduced to its residual value τ_r. Because all inelasticity has been idealized as occurring on the frictional surface, Δ includes both the actual opening of the surface due

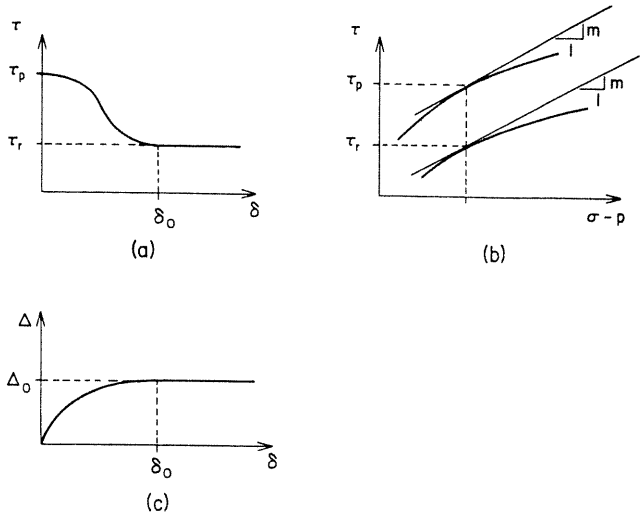

Fig. 2. Constitutive relation for the frictional surface. (*a*) For constant normal stress and pore pressure, the shear stress on the frictional surface τ decreases from a peak value τ_p to a residual value τ_r as the slip δ increases from zero to δ_0. (*b*) The level of shear stress needed to produce a given amount of slip increases with the effective stress $\sigma - p$, where σ is the normal stress and p is the pore pressure. (*c*) The uplift Δ accompanying slip increases to a maximum of Δ_0 when $\delta = \delta_0$.

to uplift and the increase in void volume due to microcracking in material adjacent to the fault surface. Specific forms for f are not well constrained by experiments, but a simple one that seems consistent with observations [*Teufel*, 1981; *Barton*, 1976] is

$$f(x) = 2x - x^2 \qquad 0 \le x \le 1 \tag{6}$$

The deformation is coupled to the movement of pore fluid by assuming that a volume of fluid equal to that of the newly created void space is drawn into the frictional surface. If the density of the pore fluid is ρ, then the mass of fluid drawn in per unit area of slip surface is $\rho\Delta$. Thus the rate of fluid mass influx q is given by

$$q = \rho\dot{\Delta} + \rho\Delta\ \dot{p}_0/K_f \tag{7}$$

where the overdot denotes the time derivative and $K_f = \rho\ dp/d\rho$ is the bulk modulus of the pore fluid. This change in fluid mass on the fault surface must be balanced by flow from the surrounding material. This flow is simply assumed to be proportional to the difference between the pore pressure on the fault surface p_0 and that in the reservoir p_1:

$$q = \rho\kappa(p_1 - p_0)/h \tag{8}$$

The permeability κ can be expressed in a more familiar form as $\kappa = k/\mu$, where k has units of area and μ is the fluid viscosity. This assumption is similar to that made by *Rudnicki* [1984]. Although it is consistent with Darcy's law for steady state flow, the relation (8) must be regarded as an ad hoc approximation. Nevertheless, in view of the simplifications that result from its adoption, the other idealizations in the problem, and the absence of detailed observational evidence, the adoption of this approximation seems warranted.

The material adjacent to the fault surface is assumed to be responding elastically. This will actually be the case if the material unloads from peak stress. However, coupled deformation diffusion can cause a slight increase in the shear stress over the drained (constant pore pressure) value τ_p. For elastic deformation, the shear stress is given by

$$\tau = \tau_p + G(U - \delta)/h \tag{9}$$

where G is the elastic shear modulus governing unloading. Because equilibrium requires that the shear stress be uniform in the slab, the stress given by (9) must be equal to that given by (4). Equating these expressions yields

$$U = \delta - [(\tau_p - \tau_r)h/G]g(\delta/\delta_0) + (hm_0/G)[\sigma - (p_0 - p_1)] \tag{10}$$

Equating (7) and (8) yields

$$\kappa(p_1 - p_0)/h = \dot{\Delta} + \Delta\ \dot{p}_0/K_f \tag{11}$$

For simplicity, we will first consider the response for the normal stress prescribed as constant. In this case $\sigma = 0$ because σ is the deviation of the normal stress from its value when $\tau = \tau_p$. Later changes in σ are prescribed to simulate those that occur in the axisymmetric compression test. Also the shear displacement U will be assumed to increase at a constant rate $\dot{U}_0$. With these simplifications, (10) can be written in nondimensional form as

$$T = Y - (2A/3)g(Y) + P \tag{12}$$

where $Y = \delta/\delta_0$, $T = \dot{U}_0 t/\delta_0$, $P = m_0 h(p_1 - p_0)/(G\delta_0)$, and $A = 3(\tau_p - \tau_r)h/2G\delta_0$. Similarly (11) can be rewritten as

$$2P = \varepsilon f'(Y)(dY/dT) - \varepsilon\alpha f(Y)(dP/dT) \tag{13}$$

where $\varepsilon = \dot{U}_0 t_D/\delta_0$, $t_D = 2\Delta_0\ m_0\ h^2/(\delta_0\kappa G)$, and $\alpha = G\ \delta_0/(m_0 h K_f)$. A detailed discussion of the significance and numerical values of these nondimensional parameters will be given in a later section. However, note that for $g(x)$ given by (3), the nondimensional parameter A is the ratio of the largest magnitude of the slope of the drained τ versus δ relation to the unloading stiffness (G/h) of the surrounding material. Thus A is larger if the shear stress decreases more rapidly with slip or if the surrounding material is more compliant.

Equations (12) and (13) can be combined as follows:

$$\varepsilon\frac{dY}{dT} = \frac{2[T - Y + (2A/3)g(Y)] + \varepsilon\alpha f(Y)}{f'(Y) + \alpha f(Y)[1 - (2A/3)g'(Y)]} \tag{14}$$

Before proceeding with the numerical results for the solution of (14), we first consider some limiting cases. These are easily obtained and serve to illustrate the character of the response.

Limiting Cases

First, consider the drained response: The imposed deformation U increases so slowly that fluid mass exchange between the frictional surface and the surrounding material prevents any change of pore pressure. Thus $p_0 = p_1$, and for constant normal stress, (10) simplifies to

$$U = \delta - [(\tau_p - \tau_r)h/G]g(\delta/\delta_0) \tag{15}$$

This equation can also be obtained from (14) by setting $\varepsilon = 0$ and using $U = \dot{U}_0 t$. If (15) is written in incremental form, the result is

$$\frac{d\delta}{dU} = \frac{1}{1 - (2/3)Ag'(\delta/\delta_0)} \tag{16}$$

Thus the ratio of the increment of slip on the fault surface to an increment of imposed shear displacement becomes unbounded when $\delta = \delta_*$, where δ_* satisfies

$$g'(\delta_*/\delta_0) = 3/2A \tag{17}$$

For $g(x)$ given by (3) this condition is met for $A \ge 1$. The value of δ_* is

$$\delta_* = (\delta_0/2)[1 - (1 - A^{-1})^{1/2}] \tag{18}$$

and the corresponding value of U is

$$U_* = (\delta_0/2)[1 - 2A/3 + (2A/3)(1 - A^{-1})^{3/2}] \tag{19}$$

There is also another value of δ satisfying (15) for the same value of $U = U_*$:

$$\delta_1 = \delta_0/2 + \delta_0[1 - A^{-1}]^{1/2} \tag{20}$$

For $g(x)$ given by (3) the drained response can be rewritten in terms of U_*, δ_*, and δ_1 as follows:

$$U = U_* + (4A/3)(\delta - \delta_*)^2(\delta - \delta_1)/{\delta_0}^2 \tag{21}$$

The drained solution has a simple graphical interpretation shown in Figure 3. Figure 3*a* shows a schematic plot of U versus δ (21). Although the entire relation is shown, U is assumed to be monotonically increasing so that only those portions are physically meaningful. The graph has a horizontal tangent at $\delta = \delta_*$ where the condition (17) is met. Figure 3*a* also indicates the availability of another solution at U_*. If $A \le 4/3$, this solution is given by δ_1; for $A > 4/3$ this solution is given by setting $g = 1$ and $U = U_*$ in (15). A naive interpretation that neglects dynamic effects would be that the slip δ

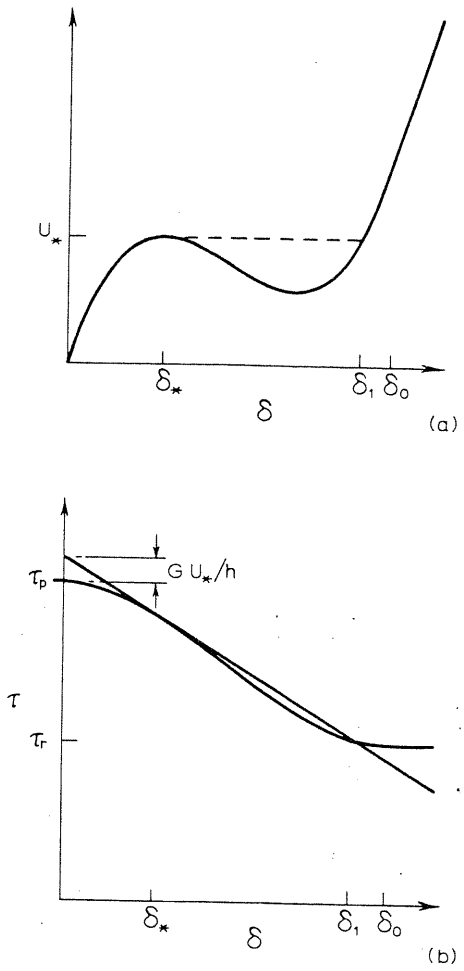

Fig. 3. Graphical interpretation of instability for drained response. (*a*) Plot of (21). Only the portion corresponding to increasing U is physically meaningful. Instability occurs when the curve has a horizontal tangent at $\delta = \delta_*$. The figure also shows the other possible equilibrium solution $\delta = \delta_1 < \delta_0$. (*b*) The drained solution is given by the intersection of the straight line of slope $-G/h$ (9) with the τ versus δ slip-weakening curve (2). Instability occurs when, as shown, the line becomes tangent to the slip-weakening curve at $\delta = \delta_*$ and $U = U_*$.

simply increases instantaneously from δ_* to δ_1 or the next equilibrium value depending on the magnitude of A. We will show that the inclusion of pore pressure alterations eliminates this instantaneous jump and allows a rapid but continuous increase in slip.

Figure 3*b* shows the corresponding plot of shear stress versus slip. The drained solution is given by the intersection of the straight line (9) and the τ versus δ relation given by (2). As shown, the condition (17) is met when these curves become tangent at $\delta = \delta_*$.

The contrasting limit to drained response is undrained response for which the deformation is imposed at a rate that is too rapid to allow time for fluid-mass exchange. Formally, the governing equation in this case can be obtained by taking the limit $\varepsilon \to \infty$ in (14). However, it is more instructive to note that for undrained conditions the left-hand side of (11) is zero. Solving for the rate of change of pore pressure yields

$$\dot{p}_0 = -K_f f'(\delta/\delta_0)\, \dot{\delta}/[\delta_0 f(\delta_0)] \qquad (22)$$

where (5) has been used. Because $f(0) = 0$, the pore pressure on the fault surface initially decreases at an infinite rate for undrained response. This unrealistic prediction is an artifact of idealizing the frictional surface as appearing instantaneously with zero width at peak stress but has little effect on the solution. Differentiating (4) and substituting (22) gives the slope of the τ versus δ relation for undrained response:

$$(d\tau/d\delta)_{\text{undrained}} = -[(\tau_p - \tau_r)/\delta_0]g'(\delta/\delta_0) + m_0 K_f f'(\delta/\delta_0)/[\delta_0 f(\delta/\delta_0)] \qquad (23)$$

The first term in this equation is the slope for drained response and the second term reflects the hardening due to the decrease in pore pressure (increase in effective compressive stress) induced by dilatancy. The hardening effect is proportional to the friction coefficient m_0 and the pore fluid bulk modulus K_f. Large decreases in pore fluid pressure can reduce K_f by allowing dissolved gases to come out of solution [*White*, 1976] or by reaching the liquid-vapor transition. In the limit of K_f falling to zero the hardening effect disppears.

Equating the right-hand side of (23) to $(-G/h)$ yields the following condition for $d\delta/dU$ to become unbounded during undrained response:

$$f'(\delta/\delta_0) + \alpha f(\delta/\delta_0)[1 - (2A/3)g'(\delta/\delta_0)] = 0 \qquad (24)$$

where $\alpha = G\delta_0/(m_0 h K_f)$. If the pore fluid is incompressible, $K_f \to \infty$ and $\alpha = 0$. For f given by (6), (24) is met only when $\delta = \delta_0$. As discussed in the next section, the value of α is approximately 0.23 if the pore fluid is liquid water and, in this case, (24) is met only for values of A greater than about 4.5. Figure 4 shows the locus of values of A and α for which (24) is met for $0 < \delta < \delta_0$.

A particularly simple case occurs when $\delta > \delta_0$. Then $g = 1$, $f = 1$, and g' and f' are zero, Thus (14) reduces to

$$\varepsilon(dY/dT) = 2[T - Y + (2A/3)]/\alpha + \varepsilon \qquad (25)$$

The solution is

$$Y = T + (1 - T_0)\exp[-a(T - T_0)] + (2A/3)\cdot\{1 - \exp[-a(T - T_0)]\} \qquad (26)$$

where $a = 2/\alpha\varepsilon$ and T_0 is the value of T when $Y = 1$ or $\delta = \delta_0$. The corresponding value of P can be obtained by substituting (26) into (12) with $g = 1$. Note that for an incompressible fluid,

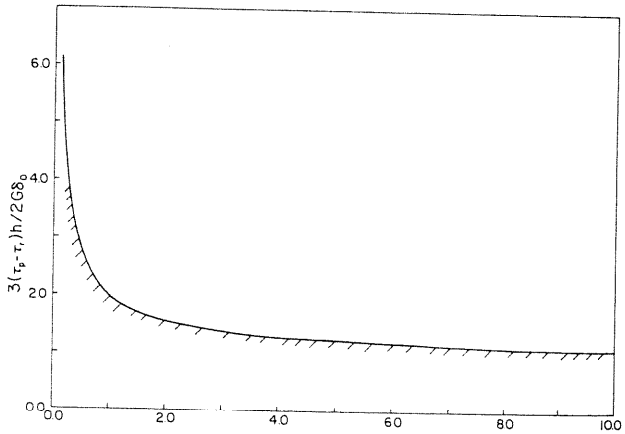

Fig. 4. The locus of values of $A = 3(\tau_p - \tau_r)h/2G\delta_0$ and $\alpha = G\delta_0/m_0 h K_f$ for which (24) is met in $0 < \delta < \delta_0$. For values of A and α below the curve (on the hatched side) there are no real roots to (24) in $0 < \delta < \delta_0$.

$K_f \to \infty$ and $\alpha = 0$. Hence (26) reduces to $Y = T + (2A/3)$ and $p_0 = p_1$.

NUMERICAL VALUES OF PARAMETERS

This section discusses the numerical values of parameters that enter the analysis. Most of them can be estimated from experiments, but as is typical, extrapolations to values appropriate to the field are uncertain.

Rice [1979, 1980] and *Wong* [1982] discuss values for a characteristic sliding distance $\bar{\delta}$ defined so that the area under the slip weakening curve in excess of τ_r is equal to $(\tau_p - \tau_r)\bar{\delta}$. This area can be identified as the shear fracture energy. For the shape of the slip-weakening curve used here (3), $\bar{\delta} = (\delta_0/2)$. From the data of *Dieterich* [1978, 1979*a*] for sliding on flat ground surfaces of Westerly granite, *Rice* [1979, 1980] infers values of $\bar{\delta}$ in the range of 0.5–10 μm. These values are 2–3 orders of magnitude lower than the value $\bar{\delta} = 0.34$ mm determined from postpeak data of *Rummel et al.* [1978] for sliding on a polished sawcut in a specimen of Fichtelgebirge granite. Still larger values, $\bar{\delta} \simeq 0.5$ mm, are inferred by *Rice* [1980] from *Rummel et al.*'s [1978] postpeak data on initially intact specimens. *Wong* [1982] has determined values of $\bar{\delta}$ from postpeak deformation of initially intact specimens of Westerly granite for several temperatures and pressures and tabulated values for a few other rock types. The values of $\bar{\delta}$ for Westerly granite range from 0.04 to 0.45 mm, with the higher values obtained at elevated temperature and pressure, and this range spans the values obtained for the Witwatersrand quartzite and Oshima granite.

Values of $\bar{\delta}$ determined from slip on flat ground surfaces increase with surface roughness, and consequently, much larger values may be appropriate in situ. *Rice* [1979] notes that a value of $\bar{\delta} = 2$ to 3 mm is consistent with the data of *Coulson* [1972] (cited by *Barton* [1973]) for "shear of a natural joint in coarse-grained granite," and *Rice* [1980] speculates that values as large as 0.1 m may be plausible for faults in the Earth.

Wong [1982] also tabulates data for $\tau_p - \tau_r$ determined from postpeak data on intact specimens. For Westerly granite at room temperature they range from 80 to 110 MPa for confining stresses from 0 to 80 MPa. At elevated temperatures, $\tau_p - \tau_r$ ranges from 50 to 150 MPa. This range spans values for other rock types considered by Wong.

For unconfined Westerly granite, *Wong* [1982] gives $\bar{\delta} \simeq 0.1$ mm, implying $\delta_0 \simeq 0.2$ mm, and $\tau_p - \tau_r \simeq 80$ MPa. To simulate laboratory experiments, the width h (Figure 1) can be taken as roughly half the specimen length or about 2 cm. Using these values with $G = 30$ GPa gives $A = 0.4$. This is smaller than the minimum value of 1.0 needed to cause instability under drained conditions, and obviously, instabilities of the type described earlier are observed in experiments. Nevertheless, as is evident from the range of data cited, there is considerable uncertainty in these values. For example, a value of δ_0 smaller by half and a smaller value of G that reflects the reduction in unloading stiffness due to cracking that occurred up to peak stress would bring A near unity. Furthermore, in assuming the shear displacement to be prescribed, we have neglected the compliance of the loading apparatus. Consequently, somewhat larger values of A, in the range of 1 2, are probably reasonable for representing laboratory experiments.

Appropriate values in situ are more uncertain. For $\delta_0 = 0.2$ m, corresponding to $\bar{\delta} = 0.1$ m speculated by *Rice* [1980], $\tau_p - \tau_r = 10$ MPa, and $G = 30$ GPa, the minimum h required for instability under drained conditions is 0.4 km. This does not seem to be an unreasonable order of magnitude, and it is possible that values of A around unity may also be representative of field conditions. Of course, slip zones in the Earth's crust are of finite length, and the effective unloading stiffness of the surrounding material decreases with the length [e.g., *Walsh*, 1971; *Rudnicki*, 1979]. Consequently, the one-dimensional model used here must be regarded as a crude approximation to slip events in situ.

The nondimensional combination α is a measure of the compressibility of the pore fluid. For liquid water, $K_f \simeq 2.2$ GPa. Using this value with $G = 30$ GPa, $m_0 = 0.6$, $\delta_0 = 0.6$, $\delta_0 = 0.2$ mm, and $h = 2$ cm yields $\alpha = 0.23$. In the analysis and calculations we have assumed that K_f is a constant, and more detailed study would take account of the dependence of K_f on pressure. However, for temperatures below 200°C, K_f is very nearly constant until the absolute pressure has been reduced to around 2 MPa, and then the reduction to very small values of K_f appropriate to the gas phase occurs very rapidly. Only for temperatures exceeding about 300°C does the transition to very small values become more gradual. (For example, see the plots given by *Anderson and Whitcomb* [1975] and *Hanks* [1974] based on the data of *Kennedy and Holser* [1966].) Consequently, it is sufficient for our purposes to model K_f as constant but to recognize that the stabilizing effects will cut off when the pore pressure on the fault has been reduced to a level near the liquid-vapor transition.

The ratio Δ_0/δ_0, which appears in t_D, is a nondimensional dilatancy factor expressing the ratio of uplift to slip. *Teufel* [1981] has measured pore volume changes associated with sliding on sawcut specimens of Coconino sandstone. He argues, on the basis of detailed microstructural observations, that the increases in pore volume are primarily due to the nucleation, extension, and opening of microcracks near the slip surface. If so, then *Teufel*'s [1981, Table 1] measurements of pore volume dilation can be converted to a dilatancy factor by dividing by the slip area and the fault displacement. This procedure yields values of $\Delta_0/\delta_0 = 0.0003$ to 0.02 with the largest values occurring for the largest confining stress. Because *Teufel*'s [1981] specimens exhibited no strength degradation, it seems likely that larger values of Δ_0/δ_0 may be appropriate to the postpeak region. The range of Δ_0/δ_0 is also consistent with *Rice*'s [1980] analysis of *Barton*'s [1973] data which yields values of at least 0.008 to 0.026. *Rice* [1980] also notes that values 2–3 times larger may result when slip is accompanied by larger strength degradation. Consequently, we use $\Delta_0/\delta_0 = 0.04$ in the calculations.

The product κG is an effective diffusivity (with dimensions of length squared per time) for exchange of fluid mass between the frictional surface and the surrounding material. *Rice and Cleary* [1976] give diffusivities inferred from laboratory measurements on six rocks. These range over 6 orders of magnitude from 0.07 cm^2/s for Charcoal granite to 1.6 m^2/s (1.6×10^4 cm^2/s) for Berea sandstone with 0.22 cm^2/s for Westerly granite. However, because of cracking that occurs prior to peak stress, somewhat larger values may pertain. *Zoback and Byerlee* [1975] measured increases in permeability of 200–400% on samples of Westerly granite stressed to between 75 and 95% of their intact peak strength. These samples had previously been loaded to high differential stress more than 20 times, and as a result, the crack porosity in these samples at the start of the experiments was about 1.5 times that measured by *Brace et al.* [1968] on intact samples. Consequently, even larger increases in permeability may occur for previously unstressed samples. On the basis of the relation between per-

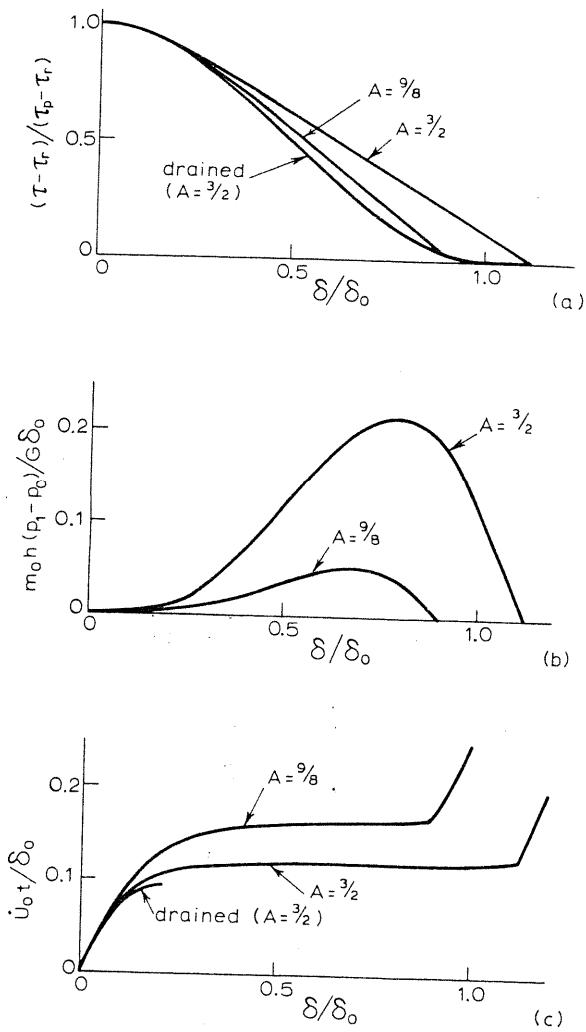

Fig. 5. Results from the numerical solution of (14) for $\varepsilon = 2 \times 10^{-3}$, $\alpha = 0.2$, and two values of A, 3/2 and 9/8. (*a*) Shear stress versus slip. The drained response for $A = 3/2$ is shown for comparison. The elevation of the stress over the drained response is due to the pressure drop shown versus slip in Figure 5*b*. (*c*) Nondimensional time versus δ/δ_0. The drained response becomes unstable at $\delta = 0.33\delta_0$ for $A = 9/8$ and at $\delta = 0.21\delta_0$ for $A = 3/2$.

meability and resistivity inferred by *Brace et al.* [1968] for Westerly granite and resistivity changes measured by *Brace and Orange* [1968], we calculate a fivefold to twelvefold increase in permeability of Westerly granite in stressing up to peak stress. Because the diffusivity is proportional to the permeability, increases in diffusivity of the same magnitude are likely.

Values of the diffusivity appropriate to field conditions near faults exhibit a similarly wide range. Values from 0.1 to 1.0 m^2/s seem to be representative, but values an order of magnitude larger or smaller are common. (See *Rudnicki* [1984] for a more detailed discussion.)

For $\kappa G = 0.2$ cm^2/s, near the value given by *Rice and Cleary* [1976] for Westerly granite, $\Delta_0/\delta_0 = 0.04$, $m_0 = 0.6$, and $h = 2$ cm, the time scale t_D is about 1 s. For larger values of κG, t_D decreases in inverse proportion. The nondimensional combination ε can be written as the product of $(\dot{U}_0/h)(h/\delta_0)t_D$. The first term $\dot{U}_0/h$ is the nominal imposed shear strain rate. For a typical laboratory experiment and, in particular, those of *Martin* [1980], $\dot{U}_0/h \simeq 10^{-6}/s^{-1}$. For $\delta_0 = 0.2$ mm, $h = 2$ cm, and $t_D \simeq 1$ s this yields $\varepsilon \simeq 10^{-4}$. For field situations a value of $\dot{U}_0/h \simeq 10^{-15}$ is representative of measured tectonic strain rates in southern California [e.g., *Prescott and Savage*, 1976; *Savage et al.*, 1981]. As discussed earlier, values of h and δ_0 are speculative, but suppose $\delta_0 = 0.1$ m and $h = 2$ km. Using $\kappa G = 0.1$ m^2/s and, again, $m_0 = 0.6$, $\Delta_0/\delta_0 = 0.04$ yields $t_D \simeq 10^6$ s and $\varepsilon \simeq 2 \times 10^{-5}$. Thus in either case, ε is much less than unity, and the range 10^{-3} to 10^{-6} is representative for both laboratory and field situations.

Analysis for Constant Normal Stress

In this section we examine the response for finite nonzero values of the imposed slip rate. Specifically, we consider U to increase at a constant rate $\dot{U}_0$. We also restrict attention for the time being to constant normal stress with $\sigma = 0$. The equation governing the slip is then (14). As already mentioned, this equation yields the drained response (15) or (21) in the limit $\varepsilon \to 0$, corresponding to very slow imposed deformation relative to the time scale of fluid-mass exchange. The smallness of ε suggests that the drained response will be a good approximation to the actual behavior until the slip rate dY/dT becomes large. This is the basis of an asymptotic analysis, which is outlined briefly in the appendix. From the earlier discussion of the drained response, dY/dT becomes unbounded at $T = T_*$, where $T_* = U_*/\delta_0$ is obtained from (19):

$$T_* = (1/2)[1 - 2A/3 + (2A/3)(1 - A^{-1})^{3/2}] \qquad (27)$$

The contrasting limit of undrained response is obtained from (14) by letting $\varepsilon \to \infty$.

The denominator in (14) is identical to the left-hand side of (24). From the discussion following (24) and Figure 4 the denominator does not go to zero for $0 \le \delta \le \delta_0$ unless α is significantly increased from its value for liquid water corresponding to a decrease in K_f. Consequently, the dilatant hardening prevents instability corresponding to an unbounded slip rate. If, however, dilatancy reduces the pressure on the frictional surface enough to cause a large reduction in K_f and a corresponding increase in α, the hardening effect vanishes and instability occurs. It is, of course, possible that the slip rate may remain bounded, but yet become large enough to be regarded as unstable. This depends on the details of the experimental apparatus, and for definiteness we continue to regard the response as stable as long as the slip rate is finite.

Although the slip rate remains bounded, dY/dT does become large, of the order of ε^{-1}. Consequently, the numerical solution of (14) requires some care. The solution was obtained for $0 < T \le T_*$ using the equation as written. However, for $T > T_*$ and $Y \le 1$, (14) was written in reciprocal form, that is, as dT/dY. This made it possible to resolve the rapid increase in Y without extremely small time steps. This also made the equations "stiff" [*Acton*, 1970; *Press et al.*, 1986], but the International Mathematical and Statistical Libraries routine DGEAR, which was used for numerical solution, has provisions for overcoming this difficulty. For $Y > 1$ the exact solution (26) was used.

Figure 5 shows results from the numerical solution of (14) for $\varepsilon = 2 \times 10^{-3}$, $\alpha = 0.2$, and two values of A, 3/2 and 9/8. Figure 5*a* shows the stress versus slip, and Figure 5*b* shows the pressure versus slip. In Figure 5*a* the drained response for $A = 3/2$ is shown for comparison. The elevation of the stress in Figure 5*a* over the drained value is due to the pressure drop shown in Figure 5*b*. Figure 5*c* shows the nondimensional time $T = \dot{U}_0 t/\delta_0$ versus slip $Y = \delta/\delta_0$. The value of T at which the

drained response becomes unstable, T_*, is 0.1389 for $A = 9/8$ and 0.0962 for $A = 3/2$. As discussed in the appendix, the asymptotic analysis suggests that for $A < 4/3$ the slip rate reaches a maximum before $\delta = \delta_0$ whereas for $A > 4/3$ the slip rate continues to increase until $\delta = \delta_0$. The solutions shown in Figure 5c appear to be consistent with this suggestion. An estimate of the maximum slip rate for $A = 3/2$ can be obtained by evaluating the right-hand side of (14) for $Y = 1$. At $Y = 1$, $T \simeq 0.12$. Using this and neglecting the term in ε yields

$$(d\delta/dt)|_{\delta=\delta_0} \simeq 0.24\delta_0/t_D\alpha$$

For $\alpha = 0.23$, $t_D \simeq 1$ s, and $\delta_0 \simeq 0.2$ mm the slip rate is about 0.2 mm/s.

The abrupt change in slope that is evident in the curves of Figure 5c (and in Figure 6c) occurs near $\delta = \delta_1$. Note that the stress rejoins the drained response curve (Figure 5a) and the pressure falls to zero (Figure 5b) at the same value of $\delta = \delta_1$. Recall that δ_1 is the other solution, in addition to δ_*, to the drained response equations at $U = U_*$ (see equations (19) and (20)). The value of δ_1 is $1.08\delta_0$ for $A = 3/2$ and $0.83\delta_0$ for $A = 9/8$. As demonstrated by the asymptotic analysis in the appendix, the change in slope is actually continuous but extremely rapid and hence appears abrupt on the scale plotted in Figure 5.

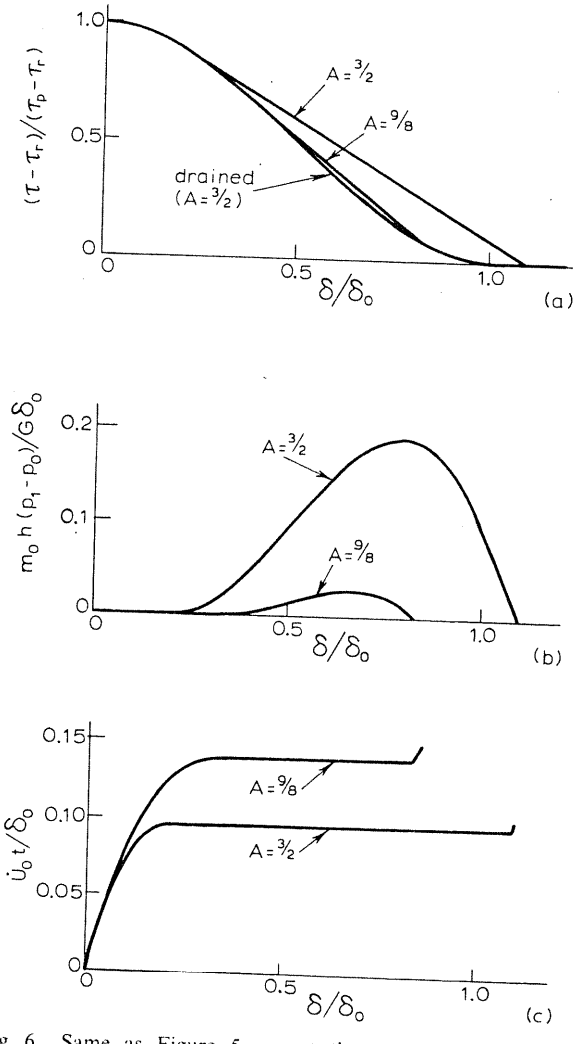

Fig. 6. Same as Figure 5, except that $\varepsilon = 2 \times 10^{-6}$. For the smaller value of ε the actual response remains closer to the drained response and in Figure 6c is indistinguishable from it on the scale shown.

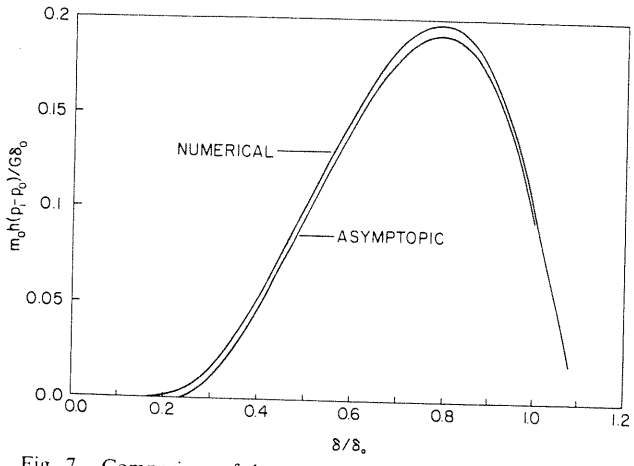

Fig. 7. Comparison of the asymptotic solution (28) for the nondimensional pressure drop to the numerical solution for $\varepsilon = 2 \times 10^{-4}$ and $A = 3/2$.

Figure 6 is the same as Figure 5 except that $\varepsilon = 2 \times 10^{-6}$. For this smaller value of ε the actual response remains closer to the drained response. Comparison of Figures 5b and 6b suggests that the maximum pressure drop is only slightly less for the smaller value of ε. Indeed, the asymptotic analysis described in the appendix (equation (A14)) yields an expression for the pressure that is independent of ε:

$$P \simeq (2/3)A(Y - Y_*)^2(Y_1 - Y) \tag{28}$$

where $Y_* = \delta_*/\delta_0$ and $Y_1 = \delta_1/\delta_0$. The maximum pressure occurs at

$$Y = (2/3)(Y_1 - Y_*) + Y_* \tag{29}$$

and is given by

$$P_{max} = (2A/3)(1 - A^{-1})^{3/2} \tag{30}$$

Figure 7 compares the asymptotic solution for the pressure to the numerical solution for $\varepsilon = 2 \times 10^{-4}$ and $A = 3/2$. As shown, the agreement is very good and improves with smaller values of ε.

Simulations of Axisymmetric Compression

In the axisymmetric compression test the normal stress on a fault inclined to the axis is not constant. However, by using a procedure similar to that of *Rice* [1980], we can introduce normal stress changes that simulate those that occur in this test. The shear and normal stresses resolved on a fault inclined at an angle of θ from the horizontal (Figure 8a) are as follows:

$$\tau = \tau_p + \tfrac{1}{2}(\sigma_a - \sigma_a^p) \sin 2\theta \tag{31}$$

$$\sigma = \tfrac{1}{2}(\sigma_a - \sigma_a^p)(1 + \cos 2\theta) \tag{32}$$

where σ_a is the axial stress, and σ_a^p is the peak value of the axial stress; as previously, σ is the alteration of the normal stress from its value when $\tau = \tau_p$. The confining stress has been assumed constant and, as a result, does not appear in these equations: it is unaltered from its value at peak shear stress. Combining (31) and (32) yields

$$\sigma = (\tau - \tau_p)(1 + \cos 2\theta)/\sin 2\theta \tag{33}$$

Substituting (33) into (4) with $p_0 = p_1$ reveals that the drained

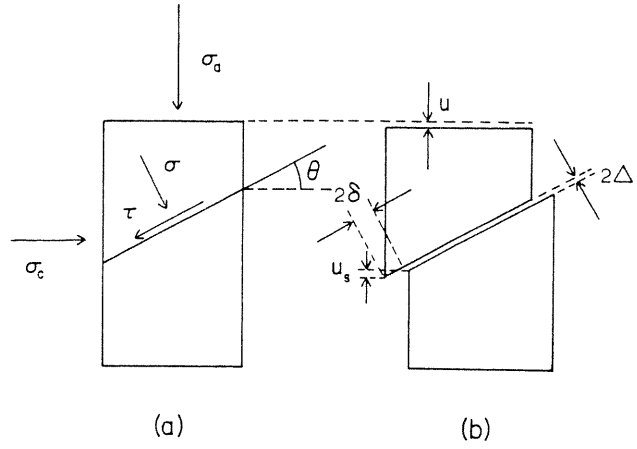

Fig. 8. Schematic illustration of the relation of stresses and slip in the axisymmetric compression test to those for the slab. (*a*) The axial stress σ_a and confining stress σ_c are related to stress σ and τ on the slip surface by (31) and (32). (*b*) The total shortening of the sample is u. The amount due to slip δ and dilation Δ is u_s(41).

response is still given by (2) with the residual stress τ_r replaced by τ_r', where

$$\tau_r' = \tau_p - (\tau_p - \tau_r)\gamma^{-1} \tag{34}$$

and $\gamma = 1 - m_0\ (1 + \cos 2\theta)/\sin 2\theta$. The lower value of the residual stress is due to the reduction in normal stress across the fault as δ increases from zero to δ_0.

Including the normal stress changes (32) makes only a minor change in the formulation. More specifically, the governing equation (14) is modified as follows:

$$\varepsilon \frac{dY}{dT} = \frac{2[T - Y + (2A/3\gamma)g(Y)] + \varepsilon\alpha f(Y)}{f'(Y)/\gamma + \alpha f(Y)[1 - (2A/3\gamma)g'/(Y)]} \tag{35}$$

This equation reduces to (14) when $\gamma = 1$. The drained response is again recovered in the limit $\varepsilon \to 0$, and instability of the drained response occurs when

$$g'(Y_*) = 3\gamma/2A \tag{36}$$

The value of Y_* and the corresponding value of T_* are as follows

$$Y_* = (1/2)[1 - (1 - \gamma A^{-1})^{1/2}] \tag{37}$$

$$T_* = (1/2)\{1 - (2A/3\gamma)[1 - (1 - \gamma A^{-1})^{3/2}]\} \tag{38}$$

The other solution to the drained response equations at T_* is given by

$$Y_1 = (1/2) + (1 - \gamma A^{-1})^{1/2} \tag{39}$$

(Recall equations (15)–(21) and Figure 3). Comparison of these expressions with those for constant normal stress ($\gamma = 1$) confirms that the reductions of normal stress are destabilizing.

Results from the numerical solution of (35) for $A = 9/8$, $\varepsilon = 2 \times 10^{-4}$, $\alpha = 0.2$, and $\gamma = 0.56$ (corresponding to $\theta = 54°$ and $m_0 = 0.6$) are shown in Figure 9. Figures 9*a* and 9*b* show the shear stress and pore pressure changes against slip δ/δ_0, and Figure 9*c* plots the nondimensional time $\dot{U}_0 t/\delta_0$ against δ/δ_0. The asymptotic solution for the pressure change is still given by (28) with the values of T_* and Y_1 from (38) and (39). Thus for the solution shown in Figure 9 the asymptotic solution predicts a maximum nondimensional pressure drop of 0.264, which agrees well with the numerical solution. Comparing this result with the corresponding ones in Figures 5*b* and 6*b* for constant normal stress demonstrates the role of the decreasing normal stress in increasing the induced pressure reduction.

The shear stress versus slip relation can be converted approximately to a postpeak curve of axial stress σ_a versus axial displacement u by assuming that all inelasticity in the postpeak region is due to slip and dilation on the fault surface. Thus σ_a is related to u by

$$\sigma_a = \sigma_a{}^p + (E/L)(u - u_s) \tag{40}$$

where E is the elastic (Young's) modulus for unloading, L is the specimen length, and u_s is the axial displacement associated with slip and dilation (Figure 8*b*). As suggested by Figure 8*b*, u_s is given by

$$u_s = 2(\delta \sin\theta - \Delta \cos\theta) \tag{41}$$

where the factor of 2 is needed for consistency with δ and Δ as defined in Figure 1. Substitution of (33) into (4) with $p_0 = p_1$ and the use of (31) yields

$$\sigma_a = \sigma_a{}^p - (\sigma_a{}^p - \sigma_a{}^r)g(\delta/\delta_0) \tag{42}$$

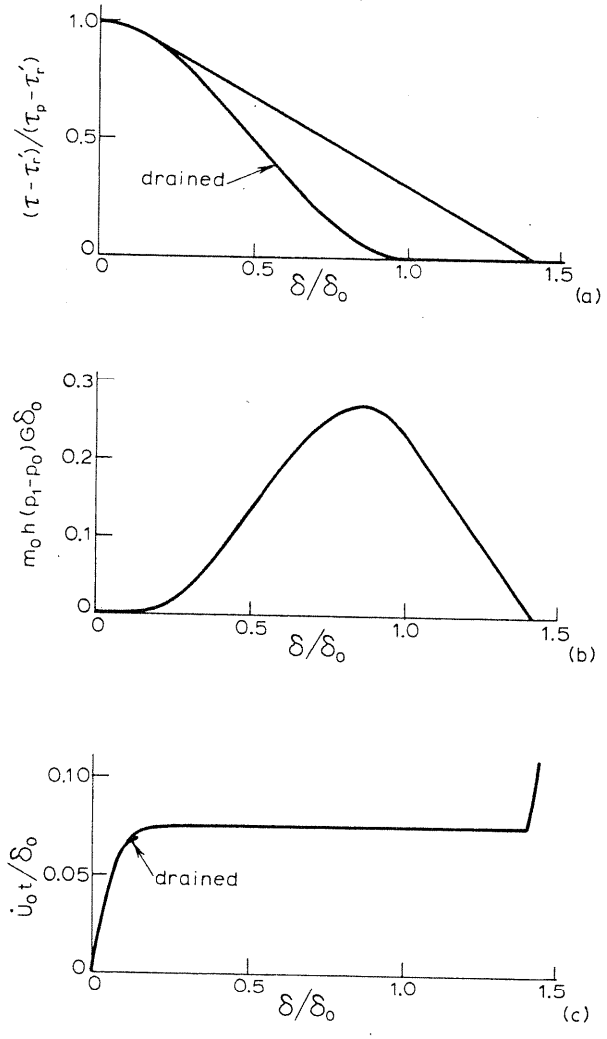

Fig. 9. Results from numerical solution of (35) for $A = 9/8$, $\varepsilon = 2 \times 10^{-4}$, $\alpha = 0.2$, $\gamma = 0.56$ (corresponding to $\theta = 54°$ and $m_0 = 0.6$). (*a*) Shear stress versus slip, (*b*) nondimensional pore pressure drop versus slip, and (*c*) nondimensional time against slip. The drained response is shown for comparison in Figures 9*a* and 9*c*.

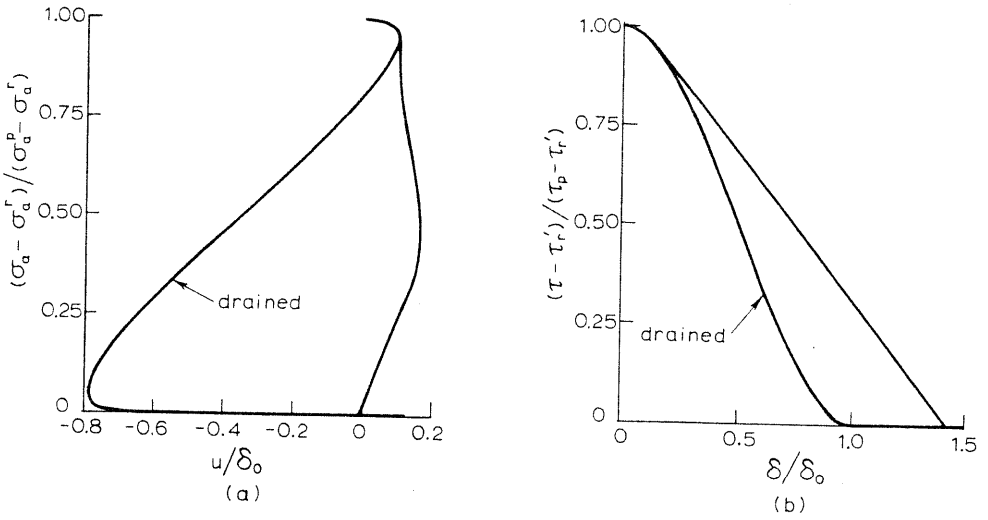

Fig. 10. Conversion of shear stress versus slip relation (Figure 10*b*) to axial stress versus axial displacement (Figure 10*a*) in a simulated axisymmetric compression test. A horizontal line gives the axial stress in Figure 10*a* corresponding to a given level of shear stress in Figure 10*b*, according to (31) and (32); $\sigma_a{}^p$ and $\sigma_a{}^r$ are the peak and residual levels of axial stress corresponding to τ_p and τ_r. The results are for the same numerical values as in Figure 9 and the conversion assumes $E = 2.5G$, $h = 0.5L$, and $N = 0.73$.

where

$$\sigma_a{}^r = \sigma_a{}^p - 2(\tau_p - \tau_r)/(\gamma \sin 2\theta) \tag{43}$$

Equations (40), (41), and (42) can be used to obtain the drained axial stress σ_a versus axial displacement relation corresponding to specified shear stress and dilatancy versus slip relations. Figure 10*a* shows the axial stress versus axial displacement relation corresponding to the shear stress versus slip relation shown in Figure 10*b*. The latter assumes $g(x)$ as in (3), and the conversion to Figure 10*a* assumes $f(x)$ as (6), $E = 2.5G$, and $h = L/2$. The condition (36) for instability of the drained response is met very slightly after the σ_a versus u curve has a vertical tangent. This difference results because the conversion of the layer problem to simulate axisymmetric compression does not correspond precisely to prescribed axial displacements.

If the response is not drained, the effect of the pore pressure on the elastic deformation must be included in (40). That is, the axial stress must be replaced by the form of the effective axial stress appropriate for elastic deformation [*Nur and Byerlee*, 1971; *Rice and Cleary*, 1976]. The result is

$$\sigma_a - (N/2)(p_1 - p_0) = \sigma_a{}^p + (E/L)(u - u_s) \tag{44}$$

where the coefficient $N \simeq 1 - E/E_s$ and E_s is a modulus of the order of that for the solid constituents. Because the pore pressure is not homogeneous in the specimen, the average pore pressure has been used in obtaining (44). Using this assumption and noting that $p_0 = p_1$ when $\sigma_a = \sigma_a{}^p$ yields (44). With the inclusion of pore pressure (42) becomes

$$\sigma_a = \sigma_a{}^p - (\sigma_a{}^p - \sigma_a{}^r)[g(\delta/\delta_0) - 3P/2A] \tag{45}$$

Equations (44) and (45) can be used to convert the solution of the layer problem to a simulation of axial stress versus axial displacement. Figure 10*a* shows the result for the solution in Figure 9. The stress versus slip solution in Figure 9*a* is included in Figure 10*b* for comparison. Although the simulation of axially symmetric compression is by no means precise, Figure 10*a* does suggest that the induced pore pressure can have a dramatic effect on the postpeak response. In particular, the pore pressure can cause an apparent change in the postpeak behavior from class II (positive postpeak slope) to class I (negative postpeak slope) [*Wawersik and Fairhurst*, 1970]. The postpeak response curve does, however, have a vertical tangent indicating that even deformation with prescribed displacement loading would be unstable. In contrast, the analysis of the layer problem indicates that instability, in the sense of an unbounded slip rate, does not occur. The cause of these differences is that the conversion of the layer solution to a simulation of axisymmetric compression does not result in prescribed axial displacement.

APPLICATION TO MARTIN'S OBSERVATIONS

Part of the motivation for this study is the discrepancy of a previous analysis [*Rudnicki*, 1984] with observation by *Martin* [1980] of pore pressure stabilization of failure in Westerly granite. Consequently, in this section we discuss Martin's observation in relation to the results of the present study.

Martin [1980] performed axisymmetric compression tests on water-saturated samples of Westerly granite. The samples were connected to a reservoir of pore fluid maintained at constant pressure. Experiments were conducted for different values of the ratio of reservoir pore pressure to confining stress, the effective confining stress, and the nominal strain rate. *Martin* [1980] classified failure as stable if the stress drop was gradual and inaudible and was preceded by gradually accelerating displacement rate over a period of several hundred seconds. Failures were designated as unstable if the stress drop was abrupt and audible, and the acceleration of the displacement rate occurred rapidly over a period of less than 20 s. Using this classification, *Martin* [1980] found that failures were stable below a critical value of the ratio of pore pressure to confining stress. This value decreased with increasing effective confining stress and decreasing nominal strain rate.

A detailed quantitative comparison with Martin's observations is not possible for several reasons. One is the qualitative nature of Martin's distinction between stable and unstable failure. Here, slip is regarded as stable if the slip rate remains

bounded. However, as already noted, it is possible that an event with large but bounded slip rate could be regarded as unstable in an experiment. Also, although the samples in Martin's experiments were deformed at a nominally constant strain rate (or, equivalently, a constant displacement rate), ranging from 6×10^{-7} s^{-1} to 2×10^{-9} s^{-1}, it is evident from Figure 1 of *Martin* [1980] that the actual strain rates departed from nominal values near failure. Furthermore, as *Martin* [1980] remarks, the results are dependent on the stiffness of the apparatus. The analysis here assumes a constant displacement rate and hence takes no account of machine stiffness. This could be included (although no value is given by *Martin* [1980]) by imagining the loading of the upper surface to be applied through a spring. The effect would be to decrease the stiffness of the material surrounding the slip surface and could be incorporated approximately by increasing the value of A. However, in view of the uncertainty about the value of A and the absence of information concerning the machine stiffness cited in *Martin* [1980], this would seem to be an unnecessary refinement at this stage.

In spite of these difficulties some comparisons can be made. *Martin* [1980] observed a dependence of the nature of failure on the value of the pore pressure in the reservoir. This feature is predicted by the present analysis. Here, dilatant hardening always stabilizes failure provided that the pressure in the reservoir is high enough to prevent reduction of the pore pressure on the slip surface to a value at which K_f decreases abruptly. The maximum pressure reduction induced by dilatant hardening is given by (A15) of the appendix. When converted to dimensional quantities, this equation is as follows:

$$p_1 = p_0 + (2/3)(\tau_p - \tau_r)m_0^{-1}(1 - \gamma/A)^{3/2} \tag{46}$$

If p_0 is given a value at which K_f abruptly decreases, then p_1 must exceed the value given by (46) for stability. *Wong* [1982] lists values of $\tau_p - \tau_r$ from 80 to 110 MPa for Westerly granite at room temperature and confining stresses ranging from 0 to 80 MPa. Using $\tau_p - \tau_r \simeq 100$ MPa with $A = 9/8$, $m_0 = 0.6$, and $\gamma = 0.56$ yields a value of 40 MPa for the second term in (46). For water at temperatures less than about 260°C, K_f remains close to its value for liquid water (2.2 GPa) until p_0 drops to about 1 MPa (see, e.g., Figure 1 of *Hanks* [1974] based on data of *Kennedy and Holser* [1966].) Thus the contribution of p_0 is negligible, and (46) yields a minimum value of p_1 for stability of 40 MPa. *Martin* [1980] observed a transition from stable to unstable failure at ratios of the confining stress to pore pressure of about 0.5. For an effective confining stress of 100 MPa, in the middle of the range studied by *Martin* [1980], the pore pressure is also 100 MPa. This is a factor of 2.5 larger than the value predicted by (46), but considering the uncertainties involved, the agreement is reasonable. More importantly, both the analysis and observations agree in the significant role in the failure process played by the pore pressure in the reservoir.

It is interesting to note that the analysis implies that the pore fluid near the slip surface may vaporize in the unstable events. Unfortunately, this is a difficult prediction to verify because the extent of the vaporization may be confined mainly to the vicinity of the slip surface. If so, it would be very difficult to detect by methods such as wave speed travel times or resistivity measurements.

Martin [1980] observed a slight decrease in the critical value of the ratio of pore pressure to confining stress with increasing effective confining stress. In the analysis the effective confining stress plays no role because the constitutive description includes a simplified dependence of material parameters on normal stress. In particular, the difference $\tau_p - \tau_r$ is independent of normal stress because both τ_p and τ_r have been assumed to exhibit the same linear dependence on normal stress. More generally, the difference $\tau_p - \tau_r$ can be expected to decrease with effective compressive stress as the result of a transition from brittle to ductile micromechanisms of deformation. *Wong* [1986] has studied the dependence of slip-weakening parameters on normal stress, and his results indicate a slight decrease in this difference for San Marcos gabbro and a slight increase for Fichtelgebirge granite in a range for which the normal stress on the slip surface varied from about 4 to 8 MPa. Equation (46) predicts that a decrease in $\tau_p - \tau_r$ does reduce the minimum value of p_1 needed for stability. This trend agrees with *Martin*'s [1980] observations.

Martin [1980] also noted that the critical ratio of pore pressure to confining stress decreased with decreasing nominal strain rate. The asymptotic result for the pressure decrease in (30) or (46) applies for small ε, that is, for small values of the product of the nominal strain rate and the diffusion time scale, but is otherwise independent of the strain rate. However, a comparison of the peak pressure reduction in Figure 5 ($\varepsilon = 2 \times 10^{-3}$) to that in Figure 6 ($\varepsilon = 2 \times 10^{-6}$) does show a slight decrease with decreasing nominal strain rate. Thus the minimum value of p_1 needed for stability decreases with decreasing strain rate in agreement with the trend of *Martin*'s [1980] results.

The duration of the period of stabilization in the analysis of *Rudnicki* [1984] was only a fraction of a second for the most plausible values of parameters and very much shorter than the tens to hundreds of seconds observed by *Martin* [1980]. The time scale of stabilization in the present analysis is in much better agreement with *Martin*'s [1980] results. An estimate of the time delay from instability of the drained response is (from (A3) of the appendix with $X = X_\#$)

$$T_\# = T_* + 2.338\varepsilon^{2/3}(1 - Y_*)^{2/3}/[(4A/3\gamma)(Y_1 - Y_*)]^{1/3} \tag{47}$$

This expression overestimates the time delay because the maximum in the pressure reduction, at which instability is possible, occurs before $T_\#$. The next order correction can be obtained from asymptotic analysis but is of order ε and is neglected for convenience here. Equation (47) can be rearranged as follows:

$$t_\# - t_* = 2.186 t_D^{2/3}(\dot{U}_0/\delta_0)^{-1/3} \tag{48}$$

where we have used $A = 9/8$ and $\gamma = 0.56$, in (37) and (39), for Y_* and Y_1. For $\dot{U}_0/h \simeq 10^{-7}$ s^{-1} a value appropriate to the upper end of the range tested by *Martin* [1980], and $\delta_0/h = 10^{-2}$, (48) yields $t_\# - t_* \simeq 100 t_D^{2/3}$. As discussed earlier, $t_D \simeq 1$ s, and for this value the delay time $t_\# - t_* \simeq 100$ s. If t_D is reduced an order of magnitude to 0.1 s to reflect the increases in permeability due to cracking up to peak stress, then $t_\# - t_* \simeq 22$ s. For $\dot{U}_0/h \simeq 10^{-9}$ s^{-1}, at the lower end of the range considered by *Martin* [1980], the delay time is a factor of 4.6 longer, i.e., 460 and 102 s for the same values of the other parameters. These times are much longer than those calculated by *Rudnicki* [1984] and are comparable to those observed by *Martin* [1980] for his unstable events. Except for the longest value, they are 2 or more times shorter than the delay times observed for stable events.

CONCLUDING DISCUSSION

The analysis has shown that slip-induced dilatancy coupled with the flow of pore fluid can stabilize rapid slip. Only a small amount of dilatancy, corresponding to uplift of the order of a few percent of the slip, is needed. However, the stabilizing effect decreases with decreases in the pore fluid bulk modulus. Consequently, instability can occur if the pressure near the slip surface is reduced to near the liquid-vapor transition or to a point where dissolved gases come out of solution. Although there is considerable uncertainty in some of the material and transport properties entering the analysis, the calculations illustrating the stabilizing effect have been performed for values consistent with those observed in experiments. The analysis has been carried out for a slab geometry, but normal stress changes intended to simulate those that occur in the axisymmetric compression these have been included.

The analysis agrees with observations of *Martin* [1980] in predicting that a transition from stable to unstable slip can occur at a critical value of the pore pressure in the reservoir. The predicted value of the critical pressure is smaller than that observed by *Martin* [1980] by a factor of about 2.5, but considering the possible differences in the interpretation of instability, uncertainties in the precise boundary conditions that apply to Martin's experiments, and the idealizations of the analysis, the agreement is good. The predicted time scale of the failure process is also comparable to that observed by *Martin* [1980] and much longer than that in the previous analysis of *Rudnicki* [1984]. Moreover, the observed variation of the critical pressure with confining stress and with nominal strain rate is consistent with the analysis. In short, the predictions of the analysis are in reasonable agreement with Martin's observations, and despite its simplicity, the model captures the salient features of the phenomenon.

The simplicity of the analysis is made possible by several assumptions. Foremost among these is that the flow of fluid mass into the dilating frictional surface is proportional to the difference in pore fluid pressure at the surface and in the external reservoir. This is equivalent to the assumption that the flow is governed by Darcy's law under steady state conditions. For a value of the diffusivity $\kappa G = 0.2$ m^2/s, inferred by *Rice and Cleary* [1976] for Westerly granite, and a half-specimen height of $h = 2$ cm, a time scale for fluid diffusion is of the order of 20 s ($h^2/\kappa G$). This is much less than the time scale of deformation of 10^6 s corresponding to a nominal strain rate of 10^{-6} s^{-1}. However, as frictional slip occurs, the effective strain rate will be much greater than this value. A rough estimate, obtained by dividing $h = 0.2$ cm by the estimated maximum slip rate (0.2 mm/s), is 100 s. This is still 5 times larger than the 20 s estimated for the time scale of fluid mass transport. This value is likely to be an underestimate because as discussed earlier, cracking in the sample prior to peak stress can increase the diffusivity. Thus the assumption of steady state fluid mass exchange is not unreasonable. Given the paucity of observations and uncertainties in material properties, more elaborate modeling would not seem to be warranted at this time but may be worthwhile if additional observations become available.

The analysis has also idealized all inelastic effects as occurring on the frictional surface. This might seem to be a limitation on application of the treatment to finite thickness fault zones. It is not, however, if the thickness is small by comparison to other dimensions. This is often the case in laboratory specimens and generally so in situ. The critical assumption is that the response of this zone can be characterized by a relation between stress and relative slip across the boundaries of the zone. This is an important difference from the analysis of *Rudnicki* [1984], which considered a zone of finite thickness but characterized the response in terms of a relation between stress and strain of the weakened zone material. The assumption of slip on a frictional surface in the postpeak region is, however, consistent with the analysis of *Rudnicki* [1984], who found that conditions for localization of deformation were met at the peak of the (dilatantly hardened) stress-strain curve for the weakened layer material. Thus subsequent deformation was predicted to be localized within the weakened layer and hence is sensibly idealized as slip on a surface.

It is as yet an open question whether the mechanism discussed here is relevant to field processes. Although increasing confining stress might be thought to suppress dilatancy, *Teufel*'s [1981] data actually show an increase in dilatancy with confining stress, probably due to increased cracking near the slip surface. Obviously, this trend cannot continue indefinitely, but it does suggest that dilatancy may persist to depths of earthquakes. *Raleigh and Marone* [1986] in a recent study of dilatancy of quartz gouge in shear found that the onset of dilatancy is nearly independent of normal stress. They conclude that dilatancy could occur prior to earthquakes in natural fault zones.

The ambient pore pressure will increase with depth and, according to this analysis, tend to increase stability. For example, assuming hydrostatic conditions, the pore pressure at 5 km depth is about 50 MPa. In addition, the pore pressure reduction predicted by (46) will be less than for laboratory situations because of the lower values of $\tau_p - \tau_r$ thought to be appropriate to the field. For example, for $\gamma = 1$, $A = 3/2$, $m_0 = 0.6$, and $\tau_p - \tau_r = 10$ MPa the second term of (46) is only 2.1 MPa. However, as noted earlier, values of A appropriate to field conditions are largely uncertain. The larger ambient pressure and smaller pressure reductions in situ may be offset by increasing temperature with depth, which may cause significant reductions in K_f with more modest reductions in pressure. However, for a temperature gradient of 20°–25°C/km [*Henyey and Wasserburg*, 1971] the temperature at 5 km is only 100°–125°C. This is well below values at which the approximation of constant K_f with an abrupt cutoff becomes unsuitable.

The analysis also suggests that the duration of the stabilization process is sufficiently long that detection by field measurements may be possible. For example, using $A = 3/2$, $\gamma = 1$, $\dot{U}_0/h = 10^{-15}$ s^{-1}, $\delta_0/h = 0.5 \times 10^{-4}$, and $t_0 = 10^6$ s in (47) yields $t_\# - t_* \simeq 709$ days. Unfortunately, because the spatial extent of dilatancy may be limited to near the fault surface, it will be difficult to detect by methods such as wave speed time delays or resistivity. On the other hand, because the slip rate during the stabilization period is predicted to be much greater than the tectonic strain rate, this rapid slip may be detectable by ground surface measurements. Distinguishing the deformation due to dilatant hardening from among a variety of other possible mechanisms is, however, difficult.

Sibson [1985] has cited field evidence for processes similiar to those analyzed here. He has identified implosion breccias at dilatant fault jogs that he suggests are the result of severe pressure reductions due to rapid dilatancy. He argues that these pressure reductions are responsible for preventing rup-

ture propagation through the structures. The calculations here lend some support to this suggestion by demonstrating that small amounts of dilatancy can be effective in stabilizing slip. Unfortunately, the one-dimensional model used here is severely limited in its application to faults in situ, and hence a detailed analysis of *Sibson*'s [1985] proposed mechanism is not possible. Faults in situ have ends or slip only over a finite portion of their surface. Also, the stress concentration at the ends of the fault may induce dilatancy in the material surrounding the fault, and it is likely that this is the source of the dilatancy in fault stepover zones.

Although detection of dilatant hardening effects in the field may be difficult, the analysis here, *Martin*'s [1980] laboratory experiments, and *Sibson*'s [1985] observations suggest that they can be significant in stabilizing slip and rupture propagation. Further analysis is needed to assess this possibility more thoroughly.

APPENDIX: ASYMPTOTIC ANALYSIS

The presence of the small parameter ε in (14) and (35) suggests the possibility of an asymptotic analysis. The analysis of (14) is similar to that outlined by *Rudnicki* [1984]. Consequently, the analysis of (35), which includes (14) as a special case, will be described concisely here. By using (3), (35) can be written as

$$\varepsilon(dY/dT) = \{2[T - T_* - (4A/3\gamma)(Y - Y_*)^2(Y - Y_1)] + \varepsilon\alpha f(Y)\} \cdot \{f'(Y)/\gamma + \alpha f(Y)[1 - (2A/3\gamma)g'(Y)]\}^{-1} \quad \text{(A1)}$$

where Y_*, T_*, and Y_1 are given by (37), (38), and (39), respectively. As already noted, setting $\varepsilon = 0$ yields the drained response. This approximation will be suitable until the derivative dY/dT becomes large in the vicinity of T_* and overcomes the smallness of ε. This suggests that the original equation be rescaled for (Y, T) near (Y_*, T_*). The desired scaling must be consistent with the drained response for $T < T_*$ and must incorporate terms that mitigate the unbounded slip rate predicted by the drained response at T_*. On the basis of these considerations the desired scaling is

$$Y = Y_* + \varepsilon^{1/3}Z \quad \text{(A2)}$$

$$T = T_* + \varepsilon^{2/3}X \quad \text{(A3)}$$

Substituting (A2) and (A3) into (A1) and taking the limit $\varepsilon \to 0$ yields

$$\frac{dZ}{dX} = \frac{\gamma X + (4/3)AZ^2(Y_1 - Y_*)}{(1 - Y_*)} \quad \text{(A4)}$$

This equation can be reduced to the standard form of the Airy equation [*Abramowitz and Stegun*, 1964, equation 10.4.1] by using the substitutions described by *Rudnicki* [1984]. The solution is

$$Z = \frac{[\gamma(1 - Y_*)]^{1/3}}{[(4/3)A(Y_1 - Y_*)]^{2/3}} \frac{Ai'(-X/\lambda)}{Ai(-X/\lambda)} \quad \text{(A5)}$$

where

$$Ai(\pm z) = \pi^{-1}\int_0^\infty \cos(t^3/3 \pm zt)\, dt$$

is the appropriate Airy function [*Abramowitz and Stegun*, 1964], the prime denotes the derivative with respect to the argument, and

$$\lambda = (1 - Y_*)^{2/3}[(4A\gamma/3)(Y_1 - Y_*)]^{-1/3}$$

Although the solution (A5) yields a bounded slip rate at $T = T_*$ $(X = 0)$, it does become unbounded at the first zero of the Airy function. This occurs at $X = X_\# = 2.338\lambda$. Because the slip rate predicted by the original equation does remain bounded, some further rescaling is needed. By means of considerations similar to those used to obtain (A2) and (A3), the appropriate scaling is determined to be

$$\zeta = Y - Y_* \quad \text{(A6)}$$

$$\xi = (T - T_*)\varepsilon^{-1} - X_\#\varepsilon^{-1/3} \quad \text{(A7)}$$

Because ε is the ratio of the diffusion time scale to the time scale of imposed deformation, ξ is time nondimensionalized by the diffusion time. Substituting (A6) and (A7) into (A1) yields

$$d\zeta/d\xi = \{(4A/3)\zeta^2(Y_1 - Y_* - \zeta) + \gamma[\varepsilon\xi + \varepsilon^{2/3}X_\# + (\varepsilon\alpha/2)f(Y_* + \zeta)]\} \cdot [(1 - Y_* - \zeta) + 2A\alpha\zeta f(Y_* + \zeta)(2Y_* - 1 + \zeta)]^{-1} \quad \text{(A8)}$$

where (36) has been used. Letting $\varepsilon \to 0$ reduces (A8) to the following equation:

$$d\zeta/d\xi = [(4/3)A\zeta^2(Y_1 - Y_* - \zeta)][(1 - Y_* - \zeta) + 2A\alpha\zeta(Y_* + \zeta)(2Y_*\zeta)(2Y_* - 1 + \zeta)]^{-1} \quad \text{(A9)}$$

This equation can be integrated, but the result is lengthy and not very revealing. Some insight into the response can be gained by examining (A9) in the limit of an incompressible pore fluid for which $\alpha = 0$. For $A < 4/3$ it can be shown that the slip rate reaches a maximum and decreases before $\delta = \delta_0$. However, for $A > 4/3$, the slip rate continues to increase and becomes unbounded as $\delta = \delta_0$. The slip rate does not become unbounded if the compressibility of the pore fluid is finite, but the character of the solution is similar. As is evident from Figures 5*c* and 6*c*, the slip rate is diminished at $\delta = \delta_0$ for $A = 9/8$ but not for $A = 3/2$.

Further analysis of (A8) also reveals the details of the rapid change in slope evident near $Y = Y_1$ (see equation (39)) in the curves of Figures 5*c* and 6*c*. Note that for $Y = Y_1$ $(\zeta = Y_1 - Y_*)$, the right-hand side of (A9) vanishes. Hence terms that were neglected in passing from (A8) to (A9) are significant. To examine (A8) for Y near Y_1, let

$$\eta = (Y - Y_1)\varepsilon^{-q} = [\zeta - (Y_1 - Y_*)]\varepsilon^{-q} \quad \text{(A10)}$$

where q is to be chosen to retain the next order term. Substituting into (A8) reveals that $q = 2/3$. Using this in (A8), canceling the common factor $\varepsilon^{2/3}$, and letting $\varepsilon \to 0$ yields

$$d\eta/d\xi = (-b\eta + \gamma X_\#)/c \quad \text{(A11)}$$

where the constants b and c are given as follows:

$$b = (4A/3)(Y_1 - Y_*)^2$$

$$c = 1 - Y_1 + 2A\alpha f(Y_1)(Y_1 - Y_*)(Y_* - 1 + Y_1)$$

The solution of (A11) subject to the condition that $\eta = 0$ $(Y = Y_1)$ at $\xi = \xi_1$ is

$$\eta = (\gamma X_\#/b)\{1 - \exp[-b(\xi - \xi_1)/c]\} \quad \text{(A12)}$$

Computing the derivative and returning to (Y,T) variables yields

$$dY/dT = (\gamma X_\#/c\varepsilon)\exp[-b(T - T_1)/\varepsilon c] \quad \text{(A13)}$$

where T_1 is the value of T at which $Y = Y_1$. Thus as T passes through T_1 (and Y through Y_1), the derivative changes from

exponential growth to exponential decay. Because $\varepsilon \ll 1$, the rates of growth and decay are extremely large, and when Y is plotted versus T on the scale of Figures 5 and 6, it appears as if the derivative dY/dT is discontinuous.

The asymptotic expression for the pressure given in the text (28) can be obtained by using (A6) and (A7) in (12). The result, after using (3) and letting $\varepsilon \to 0$, is

$$P = (4/3)A\zeta^2(Y_1 - Y_* - \zeta) \tag{A14}$$

The maximum value of P occurs at $\zeta = (2/3)(Y_1 - Y_*)$ and is given by

$$P_{max} = (2/3)A(1 - \gamma A^{-1})^{3/2} \tag{A15}$$

Acknowledgments. Jim Rice suggested that the stabilization observed by Martin [1980] may be associated with frictional sliding after a fault formed in the sample. This study was initiated under support from the U. S. Geological Survey (USGS), Department of the Interior, under USGS grant agreement 14-08-0001-G-978, and completed with support from National Science Foundation grant EAR-8511536.

REFERENCES

Abramowitz, M., and I. A. Stegun (Eds.), *Handbook of Mathematical Functions, Appl. Math. Ser.*, vol. 55, National Bureau of Standards, Washington, D. C., 1964.

Acton, F. S., *Numerical Methods That Work*, Harper and Row, New York, 1970.

Anderson, D. L., and J. H. Whitcomb, Time-dependent seismology, *J. Geophys. Res.*, *80*, 1497–1503, 1975.

Barton, N., A model study of rock joint deformation, *Int. J. Rock Mech. Min. Sci.*, *9*, 579–602, 1972.

Barton, N., Review of a new shear strength criterion for rock joints, *Eng. Geol.*, *7*, 287–332, 1973.

Barton, N., The shear strength of rock and rock joints, *Int. J. Rock Mech. Min. Sci. Geomech. Abstr.*, *13*, 255–279, 1976.

Brace, W. F., and A. S. Orange, Electrical resistivity changes in saturated rocks during fracture and frictional sliding, *J. Geophys. Res.*, *73*, 1433–1445, 1968.

Brace, W. F., J. B. Walsh, and W. T. Frangos, Permeability of granite under high pressure, *J. Geophys. Res.*, *73*, 2225–2236, 1968.

Coulson, J. H., Shear strength of flat surfaces in rock, *Proc. U. S. Symp. Rock Mech.*, *13th*, 77–105, 1972.

Dieterich, J. H., Time-dependent friction and the mechanics of stick-slip, *Pure Appl. Geophys.*, *116*, 790–806, 1978.

Dieterich, J. H., Modeling of rock friction, 1, Experimental results and constitutive equations, *J. Geophys. Res.*, *84*, 2161–2168, 1979*a*.

Dieterich, J. H., Modeling of rock friction, 2, Simulation of preseismic slip, *J. Geophys. Res.*, *84*, 2169–2175, 1979*b*.

Dieterich, J. H., Constitutive properties of faults with simulated fault gouge, in *Mechanical Behavior of Crustal Rocks, Geophys. Monogr. Ser.*, vol. 24, edited by N. L. Carter, M. Friedman, J. M. Logan, and D. W. Stearns, pp. 103–120, AGU, Washington, D. C., 1981.

Hanks, T., Constraints on the dilatancy-diffusion model of the earthquake mechanism, *J. Geophys. Res.*, *79*, 3023–3025, 1974.

Henyey, T. L., and G. J. Wasserburg, Heat flow near major strike-slip faults in California, *J. Geophys. Res.*, *76*, 7924–7946, 1971.

Jamison, W. R., and L. W. Teufel, Pore volume changes associated with failure and frictional sliding of a porous sandstone, *Proc. U. S. Symp. Rock Mech.*, *20th*, 163–170, 1979.

Kennedy, G. C., and W. T. Holser, Pressure-volume-temperature and phase relations of water and carbon dioxide, Handbook of Physical Constants, edited by S. P. Clark, *Mem. Geol. Soc. Am.*, *97*, 371–384, 1966.

Martin, R. J., III, Pore pressure stabilization of failure in Westerly granite, *Geophys. Res. Lett.*, *7*, 404–406, 1980.

Nur, A., and J. D. Byerlee, An exact effective stress law for elastic deformation of rock with fluids, *J. Geophys. Res.*, *76*, 6414–6419, 1971.

Prescott, W. H., and J. C. Savage, Strain accumulation on the San Andreas fault near Palmdale, California, *J. Geophys. Res.*, *81*, 4901–4908, 1976.

Press, W. H., B. P. Flannery, S. A. Teukolshy, and W. T. Vetterling, *Numerical Recipes*, Cambridge University Press, New York, 1986.

Raleigh, B., and C. Marone, Dilatancy of quartz gouge in pure shear, in *Mineral and Rock Deformation: Laboratory Studies—The Paterson Volume, Geophys. Monogr. Ser.*, vol. 36, edited by B. E. Hobbs and H. C. Heard, pp. 1–10, AGU, Washington, D. C., 1986.

Rice, J. R., Pore pressure effects in inelastic constitutive formulations for fissured rock masses, in *Advances in Civil Engineering Through Engineering Mechanics*, pp. 360–363, American Society of Civil Engineers, New York, 1977.

Rice, J. R., Theory of precursory processes in the inception of Earth rupture, *Gerlands Beitr. Geophys.*, *88*, 91–127, 1979.

Rice, J. R., The mechanics of earthquake rupture, Physics of the Earth's Interior, edited by A. M. Dziewonski and E. Boschi, *Proc. Int. Sch. Phys. Enrico Fermi*, *78*, 555–649, 1980.

Rice, J. R., and M. P. Cleary, Some basic stress diffusion solutions for fluid-saturated elastic porous media with compressible constituents, *Rev. Geophys.*, *14*, 227–241, 1976.

Rudnicki, J. W., The stabilization of slip on a narrow weakening fault zone by coupled deformation-pore fluid diffusion, *Bull. Seismol. Soc. Am.*, *69*, 1011–1026, 1979.

Rudnicki, J. W., A formulation for studying coupled deformation-pore fluid diffusion effects on localization, in *Proceedings of the Symposium on the Mechanics of Rocks, Soils and Ice*, edited by S. Nemat-Nasser, pp. 35–44, American Society of Mechanical Engineers, New York, 1983.

Rudnicki, J. W., Effects of dilatant hardening on the development of concentrated shear deformation in fissured rock masses, *J. Geophys. Res.*, *89*, 9259–9270, 1984.

Rudnicki, J. W., and J. R. Rice, Conditions for the localization of deformation in pressure-sensitive dilatant materials, *J. Mech. Phys. Solids*, *23*, 371–391, 1975.

Ruina, A. L., Friction laws and instabilities: A quasistatic analysis of some dry frictional behavior, Ph.D. thesis, Brown Univ., Providence, R. I., 1980.

Ruina, A. L., Slip instability and state variable friction laws, *J. Geophys. Res.*, *88*, 10,359–10,370, 1983.

Rummel, F., H. J. Alheid, and C. Frohn, Dilatancy and fracture-induced velocity changes in rock and their relation to frictional sliding, *Pure Appl. Geophys.*, *116*, 743–764, 1978.

Savage, J. C., W. H. Prescott, M. Lisowski, and N. E. King, Strain accumulation in southern California, 1973–1980. *J. Geophys. Res.*, *86*, 6991–7001, 1981.

Sibson, R. H., Stopping of earthquake ruptures at dilational fault jogs, *Nature*, *316*, 248–251, 1985.

Teufel, L. W., Pore volume changes during frictional sliding of simulated faults, in *Mechanical Behavior of Crustal Rocks, Geophys. Monogr. Ser.*, vol. 24, edited by N. L. Carter, M. Friedman, J. M. Logan, and D. W. Stearns, pp. 135–145, AGU, Washington, D. C., 1981.

Walsh, J. B., Stiffness in faulting and friction experiments, *J. Geophys. Res.*, *76*, 8597–8598, 1971.

Wawersik, W. R., and C. Fairhurst. A study of brittle rock fracture in laboratory compression experiments, *Int. J. Rock Mech. Min. Sci.*, *7*, 561–575, 1970.

White, J. E., Elastic dilatancy, fluid saturation, and earthquake dynamics, *Geophys. Res. Lett.*, *3*, 747–750, 1976.

Wong, T.-F., Shear fracture energy of Westerly granite from postfailure behavior, *J. Geophys. Res.*, *87*, 990–1000, 1982.

Wong, T.-F., On the normal stress dependence of the shear fracture energy, in *Earthquake Source Mechanics, Geophys. Monogr. Ser.*, vol. 37, edited by S. Das, J. Boatwright, and C. H. Scholz, pp. 1–11, AGU, Washington, D. C., 1986.

Zoback, M. D., and J. D. Byerlee, The effect of microcrack dilatancy on the permeability of Westerly granite, *J. Geophys. Res.*, *80*, 752–755, 1975.

C.-H. Chen and J. W. Rudnicki, Department of Civil Engineering, Northwestern University, Evanston, IL 60208.

(Received August 10, 1987;
revised February 8, 1988;
accepted January 15, 1988.)